Published online 15 July 2022

Nucleic Acids Research, 2022, Vol. 50, No. 14 ***7925–7937***
https://doi.org/10.1093/nar/gkac601

Notch-dependent and -independent functions of transcription factor RBPJ

Tobias Friedrich [1,2], Francesca Ferrante [1], Léo Pioger[3], Andrea Nist[4], Thorsten Stiewe [4], Jean-Christophe Andrau [3], Marek Bartkuhn [2,5], Benedetto Daniele Giaimo [1,*] and Tilman Borggrefe [1,*]

[1]Institute of Biochemistry, Justus-Liebig-University Giessen, Friedrichstrasse 24, 35392 Giessen, Germany, [2]Biomedical Informatics and Systems Medicine, Justus-Liebig-University Giessen, Aulweg 128, 35392 Giessen, Germany, [3]Institut de Génétique Moléculaire de Montpellier, University of Montpellier, CNRS-UMR 5535, 1919 Route de Mende, 34293 cedex 5, Montpellier, France, [4]Genomics Core Facility, Institute of Molecular Oncology, Member of the German Center for Lung Research (DZL), Philipps-University, Hans-Meerwein-Str. 3, 35043 Marburg, Germany and [5]Institute for Lung Health, Aulweg 132, 35392 Giessen, Germany

Received March 23, 2022; Revised May 27, 2022; Editorial Decision June 15, 2022; Accepted July 05, 2022

ABSTRACT

Signal transduction pathways often involve transcription factors that promote activation of defined target gene sets. The transcription factor RBPJ is the central player in Notch signaling and either forms an activator complex with the Notch intracellular domain (NICD) or a repressor complex with corepressors like KYOT2/FHL1. The balance between these two antagonizing RBPJ-complexes depends on the activation state of the Notch receptor regulated by cell-to-cell interaction, ligand binding and proteolytic cleavage events. Here, we depleted RBPJ in mature T-cells lacking active Notch signaling and performed RNA-Seq, ChIP-Seq and ATAC-seq analyses. RBPJ depletion leads to upregulation of many Notch target genes. Ectopic expression of NICD1 activates several Notch target genes and enhances RBPJ occupancy. Based on gene expression changes and RBPJ occupancy we define four different clusters, either RBPJ- and/or Notch-regulated genes. Importantly, we identify early (*Hes1* and *Hey1*) and late Notch-responsive genes (*IL2ra).* Similarly, to RBPJ depletion, interfering with transcriptional repression by squelching with cofactor KYOT2/FHL1, leads to upregulation of Notch target genes. Taken together, RBPJ is not only an essential part of the Notch coactivator complex but also functions as a repressor in a Notch-independent manner.

INTRODUCTION

The Notch signaling pathway is highly conserved and controls developmental and differentiation processes; when dysregulated this can contribute to several diseases including cancer (1–3). The Notch signaling pathway is seemingly simple since it does not involve any second messenger. In fact, upon ligand binding, the NOTCH receptor is proteolytically cleaved releasing its intracellular domain, known as NICD (NOTCH intracellular domain). Once cleaved off from the membrane, the NICD translocates into the nucleus, associates with transcription factor RBPJ as well as coactivators MAML (MATERMIND-LIKE) and acetyltransferase EP300 and activates the expression of Notch target genes (4). The signal is terminated with the help of proteasomal degradation of the NICD; this process is tightly regulated by post-translational modifications of the NICD itself (5,6). In absence of signaling through the NOTCH receptor, RBPJ actively represses Notch target genes recruiting corepressors including SHARP (SMRT and HDACs-associated repressor protein), KYOT2 [also known as FHL1C (four-and-a-half LIM domain protein 1C) in human] and L3MBTL3 [lethal (3) malignant brain tumor-like 3, also known as MBT1 (malignant brain tumor 1)] (7). In this context, the RBPJ-associated coactivator and corepressor complexes play key roles in regulating the chromatin environment by modulating histone post-translational modifications (PTMs) as well as exchanging canonical histones with histone variants (8–14).

While several genome-wide studies have investigated the activating role of the NOTCH/RBPJ axis (15–18), the repressive function of RBPJ is far less studied. So far, derepression of *Hes1* and *Hey1* Notch target genes was shown upon depletion of RBPJ in a hybridoma mature T cell

*To whom the correspondence should be addressed. Tel: +49 641 99 47400; Email: tilman.borggrefe@biochemie.med.uni-giessen.de
Correspondence may also be addressed to Benedetto Daniele Giaimo. Tel: +49 641 99 47438; Email: Benedetto.Giaimo@biochemie.med.uni-giessen.de

line (MT) (19). Here, we make use of RBPJ depletion in the same setting to characterize the repressive function of RBPJ on a genome-wide scale. Subsequently, we profile RBPJ-dependent transcription in presence or absence of NOTCH activation. When combining localization of RBPJ with changes in gene expression, we identify four different clusters of genes regulated by RBPJ and/or NOTCH. In addition, when disrupting the RBPJ corepressor by squelching, we observe again derepression of Notch target genes.

MATERIALS AND METHODS

Cell culture and treatments

Mouse hybridoma mature T (MT) E2-10HA cells (20–22) and Beko cells were grown in Iscove's modified Dulbecco's medium (IMDM, Gibco) supplemented with 2% FCS, 0.3 mg/l peptone, 5 mg/l insulin, nonessential aminoacids and penicillin/streptomycin. 293T and Phoenix™ packaging cells (Orbigen, Inc., San Diego, CA, USA) were cultivated in Dulbecco's modified Eagle's medium (DMEM, Gibco) supplemented with 10% fetal calf serum (FCS) and penicillin/streptomycin. Cells were grown at 37°C with 5% CO_2. *Drosophila melanogaster* Schneider cells were grown in Schneider's *Drosophila* medium (Gibco 21720024) supplemented with 10% fetal bovine serum (Gibco 10270-106), Glutamine (Gibco 25030-024) and penicillin/streptomycin (Gibco) and grown at 24°C. MT cells were treated with 20 μg/ml GSI (DAPT; Alexis ALX-270-416-M025), or with DMSO as control for 24 h. MT NICD1-ER cells were induced with (*Z*)-4-hydroxytamoxifen (4-OHT) at 1 μM final concentration (Sigma-Aldrich H7904-5MG) or ethanol as control for the indicated time.

Infection of MT cells

5×10^6 Phoenix™ cells were seeded and 24 h later cells were transfected with the plasmid DNA of choice. Briefly, 20 μg of DNA were mixed with 860 μl of H_2O and 120 μl of 2 M $CaCl_2$ by vortexing. The DNA solution was transferred dropwise to 1 ml of 2× HBS buffer (50 mM HEPES pH 7.05, 10 mM KCl, 12 mM glucose, 280 mM NaCl, 1.5 mM $NaHPO_4$) while vortexing and the solution was incubated 20 min at room temperature. In the meantime, 1 μl/ml of 25 μM Chloroquine solution (Sigma-Aldrich) were added to the Phoenix™ cells and the cells were incubated for 10 min at room temperature. The DNA solution was added to the cells and after 12 h of incubation at 37°C with 5% CO_2, the medium was replaced with fresh one. After 24 h of incubation, the medium containing the retroviral suspension was filtered and 1 μl/ml of 2 mg/ml Polybrene solution (Sigma-Aldrich) were added. Fresh medium was added to the Phoenix™ cells that were kept in culture for further infections. The retroviral solution was used for spin infection of MT cells by centrifuging 45 min at 1800 rpm at 37°C. In total, four spin infections were performed over 2 days. Positively infected cells were selected with puromycin (Serva) or blasticidin (Gibco) and, eventually, GFP positivity was analyzed using a BD FACS Calibur.

Generation of CRISPR/Cas9 depleted MT cells

The *sgRbpj_2–12* and *sgRbpj_2–14* MT cell clones were previously described (19). The *sgRbpj_2–4* and *sgRbpj_2–7* MT cell clones were generated using the combination of *sgRbpj_oligo_3* and *sgRbpj_oligo_4* while the *sgRbpj_1–5* MT cell clone was generated using the combination of *sgRbpj_oligo_3* and *sgRbpj_oligo_4* as previously described (19). The sequence of the sgRNA oligos is available in Supplementary Table S8.

Constructs

All oligonucleotides used in this study are listed in Supplementary Table S8. PCR products were cloned in the pSC-A-amp/kan (Agilent Technologies 240205-5), digested with the selected restriction enzymes (New England Biolabs) and cloned into the destination vectors accordingly to Supplementary Table S9. All plasmids were analyzed by sequencing.

The pMY-BioNICD1 IRES-GFP, pMY-BioNICD1 DEP IRES-GFP and the pMIGRI Flag-NICD1-ER IRES GFP plasmids have been previously described (8). The pMY Bio-IRES Blasticidin was previously described (19). The pMY NCMXH Bio-FLAG-NICD1 WT pSV40 Puro has been previously described (23). The pcDNA-KYOT2 WT and pcDNA-KYOT2 WW192AA were a generous gift of Dr. Rhett A. Kovall (University of Cincinnati, USA) (24). The pMIGR1 GFP pSV40 Puro was generated via standard cloning procedures. The lentiCRISPR v2 was a gift from Dr. F. Zhang (25) (Addgene plasmid # 52961). The CRISPR/Cas9 guides were designed using the online tool available at http://crispr.mit.edu/. The desired 5′ overhangs were added and oligos were phosphorylated, annealed and ligated into the lentiCRISPRv2 predigested with BsmBI.

RNA extraction, RT-PCR, qPCR and RNA-Seq

Total RNA was purified using Trizol reagent (Ambion, 15596018) accordingly to the manufacturer's instructions. 1 μg of RNA was reverse transcribed into cDNA using random hexamers and M-MuLV reverse transcriptase (NEB). qPCRs were assembled with Absolute QPCR ROX Mix (Thermo Scientific, AB-1139), gene-specific oligonucleotides and double-dye probes (see Supplementary Table S8) and analyzed using the StepOne Plus Real Time PCR system (Applied Biosystem). Data were normalized to the housekeeping gene *glucuronidase β* (*GusB*).

For RNA-Seq purposes, total RNA was purified using the RNeasy Mini Kit (Qiagen #74104), the QIAshredder (Qiagen #79654) and the DNase I (Qiagen #79254) accordingly to manufacturer´s instructions. Libraries were prepared using the TruSeq® Stranded Total RNA LT-Ribo-Zero Gold kit (Illumina RS-122–2301/2) and sequenced on an Illumina HiSeq 1500 or on a NextSeq 550 with 50 bases single reads. Alternatively, libraries were prepared at Novogene and sequenced on a NovaSeq with 2 × 150 bp.

RNA-Seq analysis

Previously published datasets used in this study are listed in Supplementary Table S1. Raw sequencing files for pub-

lished and new data were analyzed within R v.4.1.2 (https://www.r-project.org/) using a custom version of the systemPipeR R/BioConductor package (26,27) including new parameter files for various tools. TrimGalore (https://github.com/FelixKrueger/TrimGalore) was used to for quality and adaptor trimming. The quality of the trimming was validated by inspection of the results obtained by the '*seeFastq*' function included in systemPipeR. Alignment against the mouse UCSC (mm9) genome (downloaded from Illumina's iGenomes) was performed using tophat v.2.1.1 (28) with '–segment-length 25 –i 30 –I 3000' parameters and stored as binary alignment map (BAM). The efficiency of the alignment (e.g. percentage of aligned reads) was validated using the '*alignStats*' function of systemPipeR. Picard tools v.2.21.9 (http://broadinstitute.github.io/picard/) was used to remove PCR duplicates. Genomic alignment's (29) '*summarizeOverlaps*' function with the filtered BAM files and the mm9 gene transfer format file (Illumina's iGenomes) was used to generate a table with read counts per gene. These tables were normalized and used to calculate differentially expressed genes using DESeq2 v.1.28.1 (30). For the NICD1-ER datasets, previously published and new RNA-seq data was merged and the batch effects were normalized using DESeq2. We identified genes as significantly deregulated when they had a $\log_2$FC > 1 or < -1 and an adjusted p-value < 0.05.

Volcano plots based DESeq2 FDR and $\log_2$FC were generated using the EnhancedVolcano (https://github.com/kevinblighe/EnhancedVolcano) package. Gene over representation analysis and GSEA was performed using a custom-made script based on the clusterProfiler (31) package or for the clustered heat map using the Metascape (32) web interface.

In the case of the GEO entry GSE148441 (33), we used the preprocessed data as available as supplementary files with containing differential gene expression expressed as log2-transformed fold change values.

Microarray analysis

The microarray data (GSE97465 and GSE69091) (34,35) were processed within R v.4.1.2. The data was downloaded using the '*getGEO*' function from the GEOquery package (36). Expression data was scale normalized and differentially expressed genes were identified using limma (37).

Preparation of nuclear extracts, whole cell extract (WCE) and Western Blotting from MT cells

Nuclear extracts (NE) from MT cells were prepared as follows. Briefly, cells were washed with PBS and resuspended in Buffer A (20 mM HEPES pH 7.9/20 mM NaCl/5 mM $MgCl_2$/10% glycerol/0.2 mM PMSF) at the concentration of 1×10^6 cells/ml. The cell suspension was incubated 20 min on ice and mixed by vortexing. After 5 min centrifugation at 4000 rpm at 4°C, the pellet was washed twice in PBS and resuspended in Buffer C (20 mM HEPES pH 7.9/300 mM NaCl/0.2% NP-40/25% glycerol/1 mM $MgCl_2$/0.2 mM PMSF/1× Protease inhibitor mix/0.3 mM DTT) at the concentration of 1×10^6 nuclei/100 µl. After 20 min of incubation on ice, the nuclei suspension was centrifuged 5 min at 13 200 rpm at 4°C and the supernatant was collected. WCE were prepared as previously described (8). Protein concentration was measured by Bradford assay (Sigma-Aldrich) and samples were boiled after adding SDS-polyacrylamide gel loading buffer. Samples were resolved by SDS-Page and analyzed by Western blotting using antibodies against GAPDH (1:1000; abcam, ab8245), GFP (1:000; Roche, 11814460001), H3 (1:1000; abcam, ab1791), NOTCH1 (1:1000; abcam, ab128076), NOTCH1 (1:1000; CST 4147), NOTCH2 (1:1000; CST 5732), NOTCH3 (1:1000; CST 5276), NOTCH4 (1:1000; CST 2423), RBPJ (1:1000; Cosmo Bio Co. Ltd, 2ZRBP2) or RBPJ (1:1000; Cell Signaling Technology, 5313S). Briefly, membranes were blocked in 5% milk, 1× TBS, 0.1% Tween-20 (TBS-T) for 1 h at room temperature and primary antibodies were diluted in 5% milk, TBS-T. After incubation over night at 4°C, membranes were washed in TBS-T, secondary antibodies against mouse (Cell Signaling, #7076S) or rabbit (Cell Signaling, #7074S) were diluted 1:5000 in 5% milk TBS-T and finally membranes were washed in TBS-T. In the case of the RBPJ Western blotting (Cosmo Bio Co. LTD, 2ZRBP2) membranes were blocked in 5% milk, 1× TBS and the antibody was diluted 1:1000 in 5% BSA, 1× TBS, 0.3% NP40. After incubation over night at 4°C, membranes were washed in 1× TBS/0.5 M NaCl/0.5% Triton X-100 and the secondary antibody against rat (Jackson ImmunoResearch, 112-035-072) was diluted 1:5000 in 5% BSA, 1× TBS, 0.3% NP-40. Membranes were washed in 1× TBS/0.5 M NaCl/0.5% Triton X-100. All membranes were finally incubated with ECL solution and chemiluminescence was detected using a Vilber Fusion FX7 system.

ChIP-Seq

Chromatin immunoprecipitation (ChIP) was essentially performed as previsouly described (38). The only modification was that chromatin from *D. melanogaster* Schneider cells was used for spike-in purposes (each 25 µg of mouse chromatin, 25 ng of *Drosophila* chromatin were used in ChIP against RBPJ transcription factor) in presence of 2 µg of anti-His2Av (Active Motif 61686) for each immunoprecipitation.

The following antibodies were used: H3K4me1 (abcam, ab8895), H3K4me3 (Diagenode, pAb-003-050), H3K27ac (Diagenode, pAb-174-050) or RBPJ (Cell Signaling Technology, 5313S).

Libraries were prepared using the Illumina TruSeq ChIP Library Sample Prep Kit SetA (Illumina, IP-202-1012), the Diagenode MicroPlex Library Preparation kit v2 (Diagenode C05010012) or the Diagenode MicroPlex Library Preparation kit v3 (Diagenode C05010001) following manufacturer's instructions with few modifications. Libraries were purified with Agencourt AMPure XP Beads (Beckman Coulter, #A63881), quantified, analyzed on an Agilent Bioanalyzer or on an Agilent Tapestation device and pooled. Finally, sequencing was performed on a HiSeq2000, a HiSeq2500 or a NovaSeq device.

ATAC-Seq

ATAC-Seq was performed with the ATAC-Seq kit (Active Motif 53150) according to manufacturer´s instructions and samples were sequenced on a NovaSeq device.

ChIP-Seq and ATAC-Seq analysis

Previously published datasets used in this study are listed in Supplementary Table S10. Quality control and trimming of ChIP-Seq and ATAC-Seq data were performed as described for the RNA-Seq analysis. For the alignment of ChIP-Seq reads bowtie2 v.2.3.5.1 (39) was used. ATAC-Seq reads were aligned using HISAT2 v.2.2.1 (40) with '–no-spliced-alignment' parameter. After removal of PCR duplicates, Peakranger v.1.18 (41) was used to call peaks on filtered ChIP-seq BAM files or MAC2 v.2.2.7.1 (42) without input was used to call peaks from ATAC-Seq BAM files. MSPC v.4.0.0 (43) was used to combine the different ChIP-seq replicates and evaluate the final 'true positive peaks'. For RBPJ ChIP-Seq in Control or BioNICD1 WT a peak had to be conserved in at least two replicates in order to get accepted as a real peak. Furthermore, we demanded that peaks of the final peak list are not overlapping with any peaks that were detectable in the RBPJ depletion or the known mm9 blacklisted regions (44). In case of ATAC-Seq data, MSPC was not needed to validate peaks due to the much better signal to noise ratios as compared to the ChIP-Seq signals. We considered peaks that were conserved in at least three replicates (based on peaks called by MACS without input) as a real peak.

Peaks were associated to the putative target genes using in house tools, which works in a comparable manner to GREAT's (http://great.stanford.edu/public/html/) basal plus extension model.

Heat maps for ChIP-Seq and ATAC-Seq were generated with BED and bigWig files using deepTool's (45) '*computeMatrix*' and '*plotHeatmap*' functions. For the comparison of RBPJ signals upon Biocontrol or BioNICD1 WT deepTool's '*bamCompare*' was used. Motif enrichment analysis was performed using MEME suite v.5.0.5. Position of RBPJ sites relative to the next TSS was calculated using ChIPseeker's (46) '*annotatePeak*' function.

To quantify the binding of different histone marks in the proximity of RBPJ peaks we expanded the ranges by 650 base pairs in both directions in order to catch the modifications that are present at the nucleosomes next to the actual RBPJ binding sites. CSAW's (47) '*windowCounts*' function with 'ext = 110, width = 10' parameters was used to bin the genome and count reads within those bins. Reads within bins that are overlapping with sites of interest (RBPJ or histone modifications) were used for the quantification of binding. In order to normalize those counts normalization factors for all BAM files were calculated. Normalization factors were calculated by acquiring the average count values of 150000 random sites from the samples.

Snapshots were generated using the Gviz (48) package within R. A four-state HMM model was trained on H3K4me1, H3K27ac, H3K4me3 ChIP-Seq and ATAC-Seq data sets using ChromHMM (49).

RESULTS

Derepression of Notch target genes upon depletion of RBPJ

In order to define the role of transcription factor RBPJ in a Notch-independent manner, we performed ChIP-Seq experiments targeting RBPJ in a mature T-cell line (MT) characterized by absence of Notch activity (8–10,19). In this system, we depleted RBPJ by using the CRISPR/Cas9 technology as previously described (19). 1753 RBPJ binding sites were identified that are no longer detectable in RBPJ depleted MT cells (Supplementary Tables S1 and S2). To further characterize the RBPJ sites, accessible chromatin regions were mapped by ATAC-Seq. As expected, almost all (1735) RBPJ sites are located within open chromatin regions (Supplementary Figures S1A, B and Tables S1 and S2) and only those 1735 sites were used for further analysis. *De novo* motif discovery using MEME-ChIP identified the RBPJ binding motif among the most significantly enriched motifs (Supplementary Figure S1C and Table S3). Additionally, the SP1 (specificity protein 1), NRF1 (nuclear respiratory factor 1) and NFYA (nuclear transcription factor Y subunit alpha) motifs were identified as strongly overrepresented (Supplementary Figure S1C and Table S3). In order to understand the transcriptional function of RBPJ, we performed RNA-Seq experiments comparing wildtype versus RBPJ-depleted MT cells (Supplementary Figure S2 and Tables S1 and S4). We identified 509 genes upregulated and 148 downregulated upon RBPJ depletion in MT cells. When combining RNA-Seq and the ChIP-Seq data, we could identify 72 genes that are differentially expressed upon RBPJ depletion and bound by RBPJ (Figure 1B). Among these, 40 genes are upregulated indicating that RBPJ, in the absence of Notch, acts as a repressor of transcription.

Genome-wide analysis of RBPJ-bound and NICD1-induced genes

Subsequently, we focused on the role of RBPJ in promoting gene expression upon activation of the Notch signaling pathway. First of all, we made use of our previously published RNA-Seq data analyzing gene expression upon expression of a (*Z*)-4-hydroxytamoxifen (4-OHT)-inducible NICD1 (referred to as NICD1-ER) or of (tagged) NICD1 wildtype (NICD1 WT) in the same cell line (8) (Supplementary Tables S1 and S4). We identified 216 upregulated and 15 downregulated in both conditions (Supplementary Figure S3A and Table S4). We reasoned that the constitutive expression of the NICD1 WT may lead to upregulation of both early and late Notch responsive genes as well as secondary targets while the NICD1-ER induction for only 24 h may lead to upregulation of only early response genes so we defined the 216 commonly upregulated genes as 'Notch target genes'. Among these 216 Notch target genes we found several Notch-associated GO terms and KEGG pathways to be statistically significantly enriched (Supplementary Figure S3B and Table S5). In order to investigate the importance of RBPJ for gene expression upon activation of the Notch pathway, we also ectopically expressed the NICD1 WT in control or RBPJ-depleted MT cells (Figure 2A) and performed RNA-Seq (Supplemen-

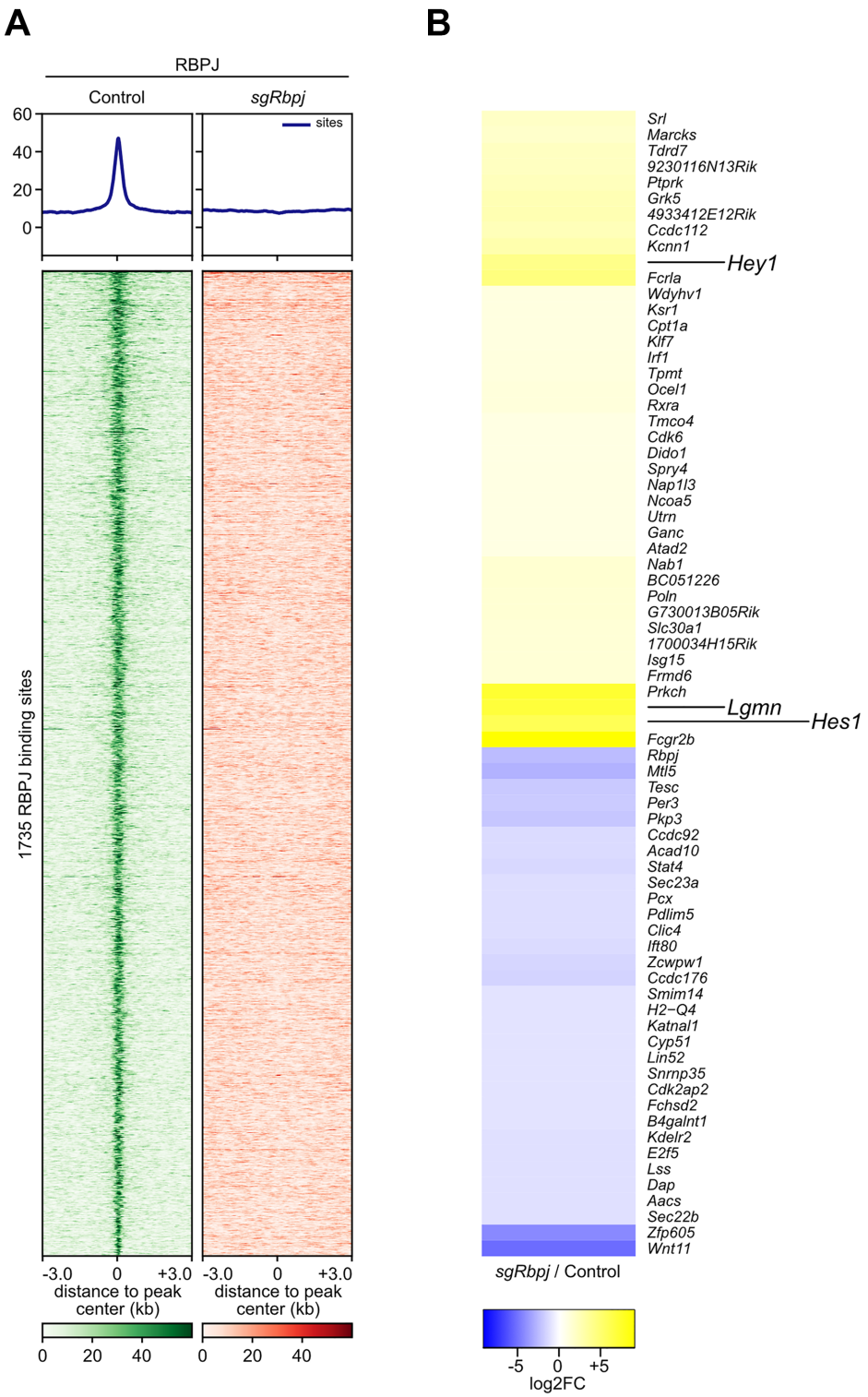

Figure 1. Identification of direct RBPJ target genes. (**A**) Genome-wide occupancy of RBPJ was investigated by ChIP-Seq in wild type or RBPJ (*sgRbpj*) depleted mature T- (MT) cells. Shown are the 1735 RBPJ sites that overlap with ATAC-Seq signal. Heat map is sorted based on the mean RBPJ binding per region over all samples. (**B**) Gene expression was analysed by RNA-Seq in wild type or RBPJ (*sgRbpj*) depleted MT cells. Heat map shows RBPJ bound genes that are significantly deregulated upon RBPJ depletion.

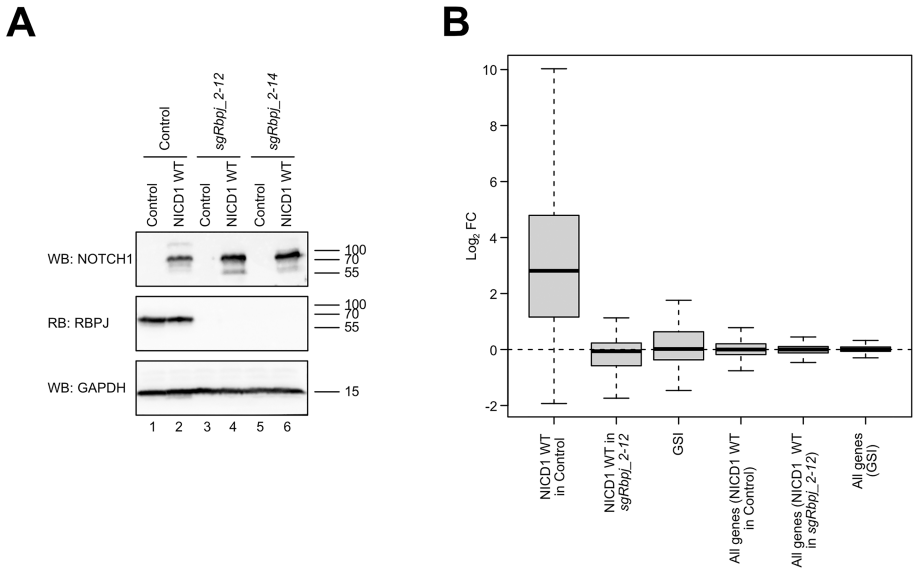

Figure 2. RBPJ is required for the Notch-dependent gene induction. MT cells control or depleted of RBPJ (clone *sgRbpj_2–12*) were infected with plasmids encoding a biotinylatable form of the NOTCH1 intracellular domain wildtype (BioNICD1 WT) or with the empty vector control (Biocontrol). (**A**) Western blotting showing that BioNICD1 WT is efficiently expressed in MT cells depleted of RBPJ (*sgRbpj_2–12* and *sgRbpj_2–14*) and control. (**B**) Box plot showing that RBPJ is required for the Notch-mediated gene induction in MT cells. Notch target genes (216 commonly upregulated genes from NICD1 WT and 24h of NICD1-ER) show no upregulation with NICD1 WT in RBPJ depleted MT cells. Additionally, the treatment for 24 h with γ-secretase inhibitor (GSI; DAPT), an inhibitor of the Notch pathway, has no effects on the expression of Notch target genes in MT cells. Effects on gene expression were analyzed by RNA-Seq.

tary Tables S1 and S4). We observed that the NICD1 WT is unable to induce Notch target genes in RBPJ-depleted cells (Figure 2B and Supplementary Table S4). Of note, the Notch pathway is not active in our MT cells since Notch target genes are not downregulated upon treatment with γ-secretase inhibitor (GSI) (Figure 2B and Supplementary Tables S1 and S4), that blocks the Notch pathway (16,23). In addition, we observed that expression of most Notch receptors (*Notch1*, *Notch3* and *Notch4*) is undetectable in MT cells, while Notch2 is expressed (Supplementary Figure S4A, B).

To better understand the effect of the Notch activation on the RBPJ occupancy, we ectopically expressed the NICD1 WT or a hypoactive NICD1 mutant defective for the interaction with EP300, termed NICD1 ΔEP (NICD1 ΔEP) (50) and performed ChIP-Seq versus RBPJ (Supplementary Tables S1 and S2). In the NICD1 WT expressing cells, we identified 3735 RBPJ binding sites that are not detectable in RBPJ-depleted cells (Figure 3A and Supplementary Table S2). Importantly, in presence of the NICD1 WT, we identified more RBPJ binding sites compared to the wild type control cells (Supplementary Figure S5A), and also enhanced RBPJ binding in presence of NICD1 WT compared to the wild type control cells (Figure 3A, B and Supplementary Figure S5B), suggesting that the NICD1 supports the binding of RBPJ to the genome as previously described (18). The increased RBPJ binding was not detectable in the NICD1 ΔEP-expressing cells (Figure 3A, B). The RBPJ binding motif was identified in the group of 3735 RBPJ binding sites together with the binding motif for SP2 (specificity factor 2), NRF1 and RUNX1 [Runt-related transcription factor 1, also known as AML1 (acute myeloid leukemia 1)] among others (Supplementary Figure S5C and Table S3).

Finally, we combined the ChIP-Seq in MT cells overexpressing the NICD1 WT with the RNA-Seq. Upon activation of the Notch pathway, we identified 65 genes that are not only upregulated by NICD1 but also bound by RBPJ (Figure 3C). Several of these genes are already known Notch target genes like *Hes1, Hey1, Il2ra, Dtx1* and *Nrarp* (Figure 3C).

Together, our analyses allowed us to identify Notch/RBPJ target genes: They are defined by (i) occupancy of RBPJ and (ii) induction by NICD1.

Genome-wide view of Notch-dependent and independent functions of RBPJ

Subsequently, we performed an integrative analysis of our ChIP-Seq and RNA-Seq data generated upon depletion of RBPJ or Notch induction. By combining both sets, we identified a total of 4307 RBPJ sites (Supplementary Figure S6). In a supervised clustering approach, we identified four different classes of genes characterized by specific RBPJ/NICD1-dependent regulatory patterns (Figure 4A and Supplementary Table S6): Cluster I is characterized by genes that are induced upon RBPJ depletion, NICD1 WT expression or 24 h of NICD1-ER induction, such as *Hes1*, *Hey1* and *Lgmn* that are well-known Notch target genes; Cluster II contains genes that are induced upon RBPJ depletion or NICD1 WT expression but not upon 24 h of NICD1-ER induction, for example *Il2ra* (interleukin 2 receptor subunit alpha, also known as CD25), a well-known Notch target gene; Cluster III represents genes induced upon NICD1 WT or 24 h of NICD1-ER but remain unchanged in RBPJ depleted setting, for example *Dtx1* and *Nrarp*, two well-known Notch target genes encoding for negative regulators of the Notch signaling pathway; Clus-

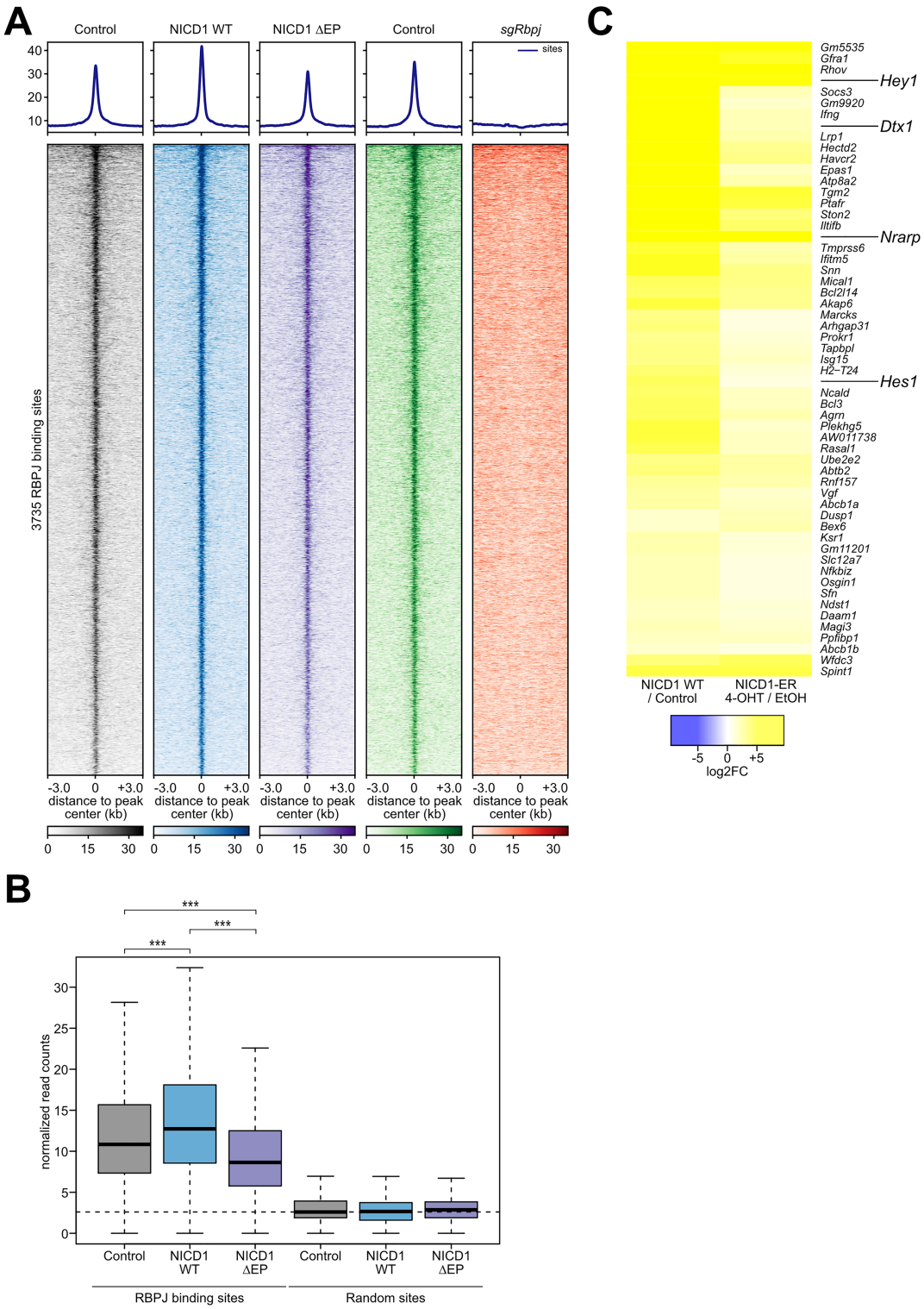

Figure 3. Notch activation increases RBPJ occupancy and supports a Notch specific transcriptional response. (**A**) Heat map shows enhanced RBPJ binding in MT cells upon Notch activation by infection with plasmids encoding a biotinylatable form of the NOTCH1 intracellular domain wildtype (BioNICD1 WT; blue), a hypoactive NICD1 mutant lacking the EP domain (BioNICD1 ΔEP; purple) or with the empty vector control (Biocontrol; grey). Additionally, wild type and RBPJ (*sgRbpj*) depleted MT cells are also shown. Heat map is sorted based on the mean RBPJ binding per region over all samples. (**B**) Quantification of the effects on RBPJ binding by Notch activation as shown in A. (**C**) Heat map showing significant expression changes of RBPJ bound genes upon activation of Notch signalling by either expression of BioNICD1 WT or induction of the NICD1-ER upon 24 h of (*Z*)-4-hydroxytamoxifen (4-OHT) treatment.

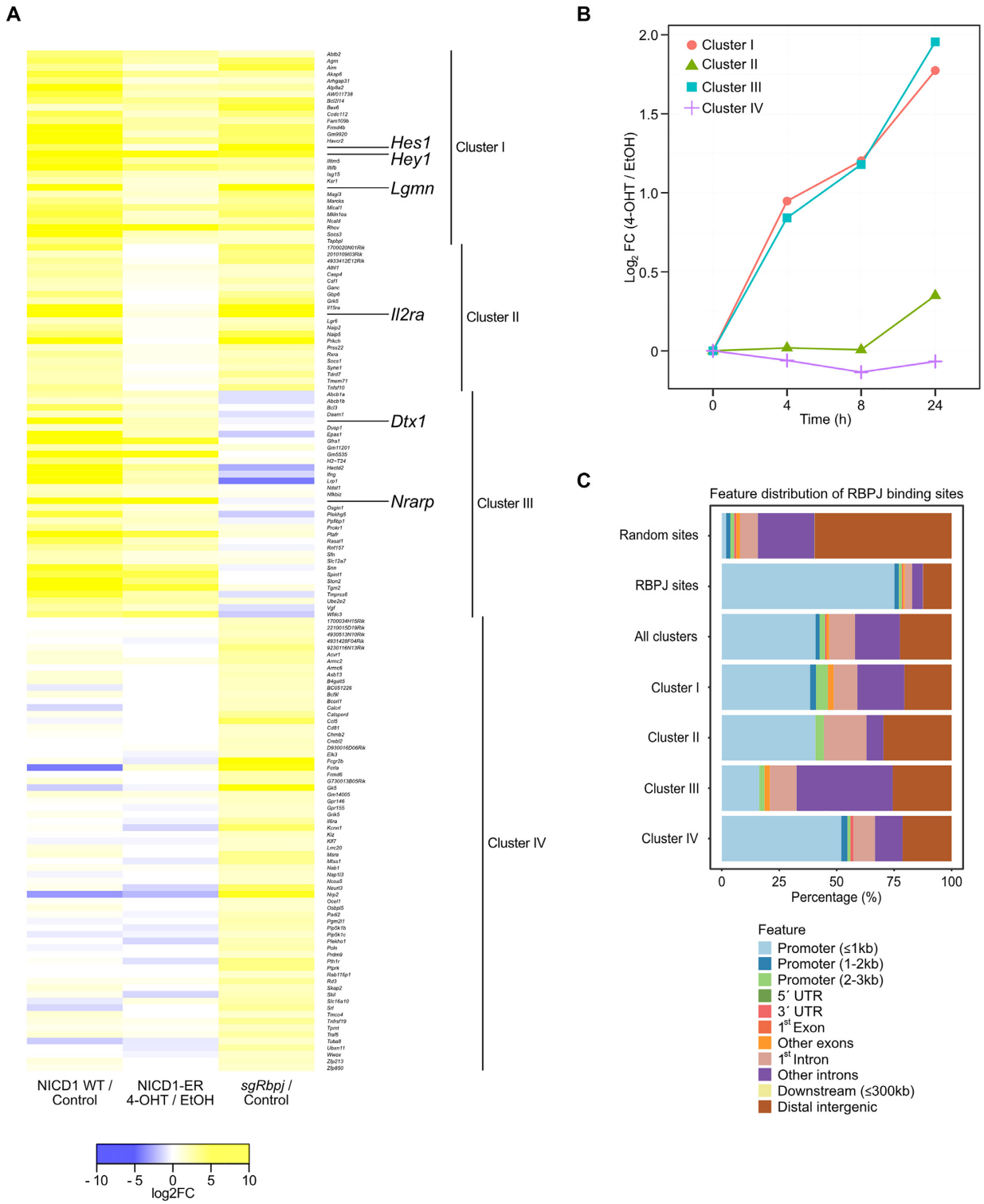

Figure 4. Four different RBPJ/Notch dependent gene clusters are revealed by integrative analysis of RBPJ occupancy and gene expression. (**A**) Heat map showing the different transcriptional responses of RBPJ bound and significantly deregulated genes either upon BioNICD1 WT infection (continuous Notch activation), 24 h (*Z*)-4-hydroxytamoxifen (4-OHT) treatment of NICD1-ER infected MT cells or in RBPJ depleted MT cells. Cluster I represents genes that are upregulated by Notch activation as well as RBPJ depletion. Cluster II contains genes that are upregulated by continuous Notch activation (BioNICD1 WT) as well as RBPJ depletion. Cluster III genes are exclusively responsive upon Notch activation. Cluster IV are genes that are unresponsive to Notch activation, but upregulated upon RBPJ depletion. (**B**) Line plot shows the average gene expression changes after different time points of 4-OHT treatment in a cluster specific manner. Genes of cluster I and III are quickly induced by activation of the Notch pathway by 4-OHT-mediated induction of NICD1-ER. Cluster III genes show only slight responsiveness after 24 h treatment and genes of the fourth cluster are generally not responsive. (**C**) Stacked bar plots showing the features associated with RBPJ binding sites. RBPJ binding sites. Overall RBPJ binding sites are predominantly associated with promoters. Within RBPJ binding sites associated with the four clusters, the sites of cluster III are the least related with promoter regions.

ter IV contains genes derepressed upon RBPJ depletion but not induced by NICD1 WT expression or 24 h of NICD1-ER. This was further validated using quantitative RT-PCR in the same clones (Supplementary Figure S7A) and also in additional independent RBPJ-depleted clones (Supplementary Figure S7B-C) as well as upon 4-OHT -mediated induction of NICD1-ER (Supplementary Figure S8).

In addition to the 24 h of NICD1-ER induction, we performed time-course experiments using the NICD1-ER expressing cells (4, 8 and 12 h) to investigate whether it is possible to further define early and late responsive Notch target genes (Figure 4B, Supplementary Figure S9 and Tables S1 and S4). While genes of clusters I and III are immediately induced upon NICD1-ER induction, genes of cluster IV are not responsive (Figure 4B, Supplementary Figure S9 and Table S4). Importantly, genes from cluster II are weakly induced only at 24 h of treatment (Figure 4B, Supplementary Figure S9 and Table S4), and this cluster includes *Il2ra*, a key receptor modulating T-cell development and also positive autologous feedback regulation. Of note, cluster I includes *Hes1* and *Hey1* that encode for transcriptional repressors while cluster III includes *Dtx1* and *Nrarp* that encode for two different negative feedback regulators of the Notch signaling pathway. Additionally, we validated these results by qPCR by ectopically expressing the NICD1 WT in RBPJ-depleted cells or in control cells and we observed that genes of clusters I, II and III require RBPJ to be induced by Notch (Supplementary Figure S10). In order to validate the relevance of the identified cluster specificities, we monitored the corresponding gene expression in publicly available data sets. Genes of cluster I and III are both induced by NICD1 in two different contexts, in T6E acute lymphoblastic leukemia cells and in small cell lung cancer (SCLC) (Supplementary Figure S11A, B) as well as downregulated in primary T cells depleted of both *Notch1* and *Notch2* (Supplementary Figure S11C, D), supporting the strong dependency of genes of clusters I and III on Notch.

Furthermore, we investigated whether positioning of enhancer relative to the transcriptional start site (TSS) of target genes matters in regard to RBPJ/NICD1-responsiveness. We observed that in general many RBPJ binding sites are in close proximity to the TSS (Figure 4C and Supplementary Figure S12A). Cluster III, containing well-known feedback regulators of the Notch response (*Dtx1* and *Nrarp*), display the enhancer sites that are most far away from TSSs (Figure 4C and Supplementary Figure S12A). One interpretation is that genes coding for feedback regulators have a characteristic enhancer positioning, making them possibly less dependent on RBPJ-mediated repression. MEME analysis identified the RBPJ binding motif among the significantly enriched motifs in clusters I, III and IV but not in cluster II (Supplementary Figure S12B and Table S3). Finally, we observed that genes in cluster I are associated with GO terms related to development. In contrast, genes in cluster II are associated with GO terms related to immune response similarly to genes in clusters III and IV (Supplementary Figure S12C and Table S7). In addition, genes in cluster IV are associated with GO terms related to the transforming growth factor beta (TGFβ) (Supplementary Figure S12C and Table S7).

For further characterization of the clusters, we performed ChIP-Seq for selected histone marks (H3K27ac, H3K4me3 and H3K4me1) in order to study the RBPJ/NICD1-dependent chromatin dynamics (Supplementary Table S1). We defined four different chromatin states based on chromatin accessibility, H3K4me1, H3K27ac and H3K4me3: State 1 represents distal enhancers displaying preferential enrichment for H3K4me1 while cluster 4 represents proximal enhancers showing a preferential enrichment for H3K4me3 (Supplementary Figure S13A). State 2 represent an intermediate state between 1 and 2 (Supplementary Figure S13A). Based on this, we observed that RBPJ sites associated with genes in cluster IV are preferentially enriched for state 4 and poorly enriched for states 1 and 2 while Clusters I, II and III are preferentially enriched for states 1 and 2 (Supplementary Figure S13A). Generally, depletion of RBPJ resulted in a slight decrease in H3K27ac and a mild increase in H3K4me3 and H3K4me1 at the RBPJ binding sites (Supplementary Figure S13B). When inspecting the individual clusters, we observed increased chromatin accessibility, H3K27ac and H3K4me3 upon RBPJ depletion at the RBPJ binding sites associated with cluster I whereas H3K4me1 remained constant (Supplementary Figure S13C–F). Cluster II featured a slight but significant increase in chromatin accessibility, H3K27ac and H3K4me3 and again no changes in H3K4me1 (Supplementary Figure S13B–F). In cluster III depletion of RBPJ led to an increase of H3K4me1 whereas chromatin accessibility, H3K27ac and H3K4me3 remained unchanged (Supplementary Figure S13B–F). Finally, cluster IV was characterized by increased chromatin accessibility, H3K27ac, H3K4me3 and H3K4me1 upon RBPJ depletion (Supplementary Figure S13B–F). Some representative examples are shown for *Hes1* (cluster I), *Dtx1* (cluster III) and *Kcnn1* (cluster IV) (Supplementary Figure S13G–I).

We have previously shown that the histone variant H2A.Z acts as a repressor of Notch target genes (8). In line with this, genes in clusters I, II and IV, which are derepressed upon RBPJ depletion, are strongly upregulated upon H2A.Z depletion. As expected, this is not the case for genes of cluster III (Supplementary Figure S13J and Tables S1 and S4).

Together, RBPJ depletion in MT cells correlates with increased H3K27ac and with minor alterations in regard to other histone marks.

Ectopic expression of KYOT2 results in derepression of Notch target genes

As an alternative to depletion of transcription factor RBPJ using CRISPR/Cas9, we aimed to disrupt the RBPJ-associated corepressor by ectopically expressing RBPJ-binding cofactor KYOT2, which is harboring a WxP motif commonly found in RBPJ-interacting proteins (22). KyoT2 is also not expressed in our MT cells, whereas other RBPJ-corepressors like SHARP and L3MBTL2 are expressed. In order to squelch away RBPJ-associated corepressors, we ectopically expressed either KYOT2 WT or the RBPJ-interacting defective WW192AA mutant (KYOT2 WW/AA) in MT cells (Figure 5A and Supplementary

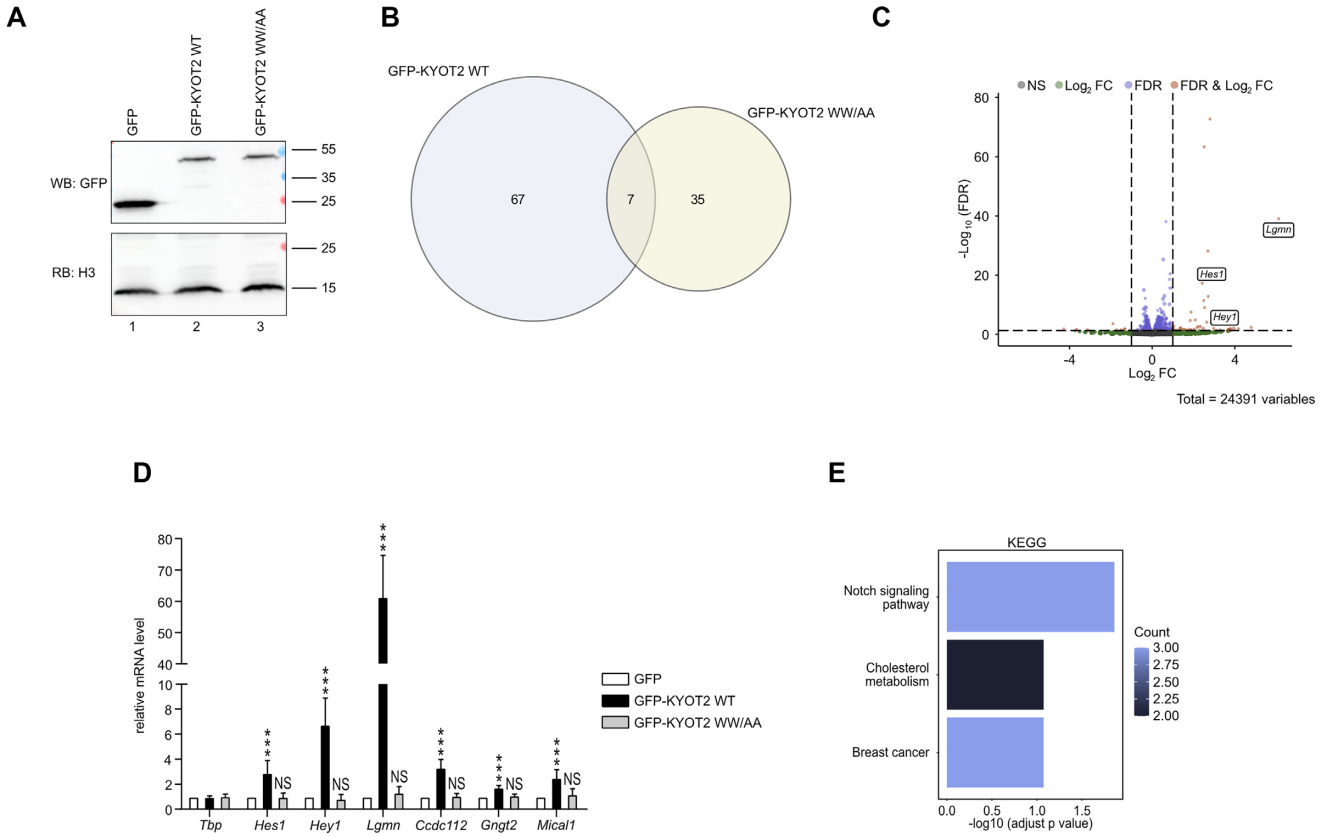

Figure 5. Ectopic expression of RBPJ binding protein KYOT2/FHL1 results in derepression of a subset of Notch target genes. (**A**) Western blot showing the expression of GFP-tagged KYOT2 wildtype (WT) and of GFP-tagged RBPJ binding defective KYOT2 mutant (KYOT2 WW/AA) in mature T (MT) cells. (**B**) Venn diagram representation of the overlap between significantly deregulated genes upon ectopic expression of GFP-tagged KYOT2 WT or GFP-tagged KYOT2 WW/AA mutant in MT cells. (**C**) Volcano plot visualizes the effects on gene expression upon ectopic expression of GFP-tagged KYOT2 WT versus GFP-tagged KYOT2 WW/AA mutant in MT cells. (**D**) Validation of the RNA-Seq data by qPCR. MT cells were infected with plasmids encoding for GFP-tagged KYOT2 WT, GFP-tagged KYOT2 WW/AA mutant or with the GFP empty vector control (control). Shown is the mean ± SD of nine independent experiments (***$P < 0.001$, [NS] not significant; unpaired Student's *t*-test). (**E**) Bar plot showing the results of the over representation analysis based on the KEGG database. The KEGG pathway 'Notch signaling pathway' is significantly enriched upon ectopic expression of KYOT2 WT but not of KYOT2 WW/AA mutant.

Figure S14A). KYOT2 WT and KYOT2 WW/AA are equally expressed as demonstrated by Western blotting (Figure 5A). We reasoned that the KYOT2 WT but not the KYOT2 WW/AA mutant would interfere with the repressive activity of the endogenous RBPJ-associated corepressor (Supplementary Figure S14A). Transcriptomic analysis showed significant differences in the gene expression levels upon ectopic expression of KYOT2 WT or KYOT2 WW/AA mutant with only 7 genes commonly deregulated by both constructs (Figure 5B, C). We first validated the results of our RNA-Seq by RT-qPCR looking at genes that are upregulated by KYOT2 WT but not by KYOT2 WW/AA mutant (Figure 5D). Among the deregulated genes, KEGG pathways and GO terms related to Notch signaling were amongst the most significantly enriched functions, confirming the ability of KYOT2 to interact with RBPJ at Notch target genes (Supplementary Figure S14B and Table S5). Similarly, GSEA identified Notch-related terms (Figure 5E and Supplementary Figure S14C and Table S5). Filtering for RBPJ-bound genes that are differentially deregulated upon ectopic expression of KYOT2 WT we identified Notch target genes *Hes1* and *Hey1* (Supplementary Table S4). Together, KYOT2 WT but not KYOT2 WW/AA mutant is able to interfere with the RBPJ-associated corepressor complex at Notch target genes.

DISCUSSION

Our study elucidates genome-wide the molecular mechanism of transcription factor RBPJ in the absence and presence of Notch coactivator. By depleting RBPJ and expressing activated Notch in presence and absence of RBPJ, we define gene clusters that are RBPJ- and/or Notch-dependent. The observed derepression upon RBPJ depletion is widespread, including several known Notch target genes.

Our study is in line with previously published data showing that the binding of RBPJ is stabilized by active Notch signal (17,18) and that it occurs on open chromatin (51), indicating Notch-dependence. However, our data also reveals that RBPJ can also act in a Notch-independent manner. There are RBPJ-bound genes, that are repressed by RBPJ-

corepressor but do not respond to Notch activation (cluster IV genes).

Cluster I and cluster III genes immediately respond to Notch, whereas cluster II genes respond weaker and later. Cluster I is characterized by genes induced upon RBPJ depletion as well as by Notch-induction, cluster III genes are induced by Notch but not upon RBPJ depletion. Cluster II are late-responsive genes that are induced upon RBPJ depletion or NICD1 expression but not upon 24 h of NICD1-ER induction. The reason for these kinetic differences remains unclear. One possible scenario is that additional transcription factors stabilize the RBPJ/NICD1 coactivator complex at genes of cluster I and III, whereas this is not the case for cluster II genes. Another option is that possibly tandemly repeated RBPJ sites allow cooperative binding of two RBPJ/coactivator complexes as previously reported for cluster I gene *Hes1* (35). Interestingly, genes in cluster IV are not induced by Notch but repressed by RBPJ. This could be explained by a scenario in which the RBPJ corepressor can form a repressive structure, possibly supported by other transcription factors or chromatin marks, that no longer allows activation by Notch. It remains to be seen, whether cluster IV genes are truly Notch-independent or whether they are Notch-induced in other cell types.

Interestingly, clusters I and II include several known Notch targets such as *Hes1*, *Hey1* and *Il2ra* (52) while negative feedback regulators of the Notch response, such as *Nrarp* and *Dtx1* (53–56), are members of cluster III. In addition, clusters I and II include *Socs1* and *Socs3* that encode for regulators of cytokine signaling that have been previously linked to the Notch signaling pathway (57,58). Our data provide a molecular explanation of the differentiation block observed at early stages of T cells differentiation upon loss-of-function of *Socs1* and *Socs3* (59) which we identify as downstream targets of the Notch signaling pathway that is well known to be essential for the early stages of T cells development (60,61). Interestingly, cluster III includes *Lrp1* which encodes for a positive regulator of the Notch response (62,63) furthermore marking the point that genes in cluster III may be required to ensure the control of the Notch response. The observation that genes in cluster IV, such as *Ccl5*, *Klf7* and *Padi2*, have been previously described to correlate positively or negatively with Notch activation (64–66) would suggest that those genes are regulated by Notch in a cell-type and/or tissue-specific fashion. However, why these genes are insensitive to Notch activation remains unclear and this aspect needs to be further investigated. One scenario is that RBPJ regulates gene expression in conjunction with an additional transcription factor and/or RBPJ requires an additional cofactor, expressed later on, to become Notch-responsive again. Promoter architecture, for example distance of the enhancer to the TSS, or chromatin context could also contribute to Notch-responsiveness.

Our data reveal in a genome-wide approach that RBPJ not only binds but also represses transcription in the absence of Notch. Previously, it was shown that RBPJ together with HDAC-containing corepressors is able to mediate transcriptional repression, terminating NICD/EP300-mediated transcriptional activation (9).

Our study is in line with previous data that have shown the dependence on different Notch receptors during T-cell development (33): Early response genes (clusters I and III) are significantly downregulated upon *Notch1*/*Notch2* depletion compared to genes in clusters II and IV and this downregulation is stronger in Phase 1 T-cells (DN1 and DN2a stages) compared to Phase 2 T cells (DN2b and DN3 stages). There are studies that RBPJ is only needed as part of the NICD-associated coactivator complex (18). In addition, conditional knockout of RBPJ and Notch also displayed very similar phenotypes in regard to T-cell development (61,67). On the other hand, biochemically, several transcriptional corepressors have been described to directly interact with RBPJ. Their *in vivo* significance as well as their Notch-related phenotypes have been confirmed by several different groups including ours. The interactions between RBPJ and corepressors are further supported by unbiased proteomic screens (14). Only in the last few years, several studies appeared demonstrating a Notch-independent *in vivo* function of RBPJ in angiogenesis (68,69) and vascular permeability (38) and a tumor suppressive role of RBPJ has been postulated in certain cancers such as breast cancer (70).

Our genome-wide study supports the notion, that the Notch-independent function of RBPJ is more widespread than previously thought affecting many genes. In future, this Notch-independent *in vivo* functions of RBPJ need to be further elucidated.

DATA AVAILABILITY

All the data generated in this study have been deposited at GEO under accession number GSE189648.

SUPPLEMENTARY DATA

Supplementary Data are available at NAR Online.

ACKNOWLEDGEMENTS

We are grateful to T. Schmidt-Wöll for excellent technical assistance. We want to thank Dr Rhett A. Kovall (University of Cincinnati, USA) for providing us with plasmids. The authors wish to acknowledge Centro de Análisis Genómico (CNAG-CRG), Spain, for sequencing the ChIP samples.
Author contributions: T.F. performed the bioinformatics analysis. F.F., L.P., K.H. and B.D.G. performed experiments. A.N. and T.S. sequenced most of the RNA-Seq samples. J.C.A., M.B., B.D.G. and T.B. supervised the work. B.D.G. and T.B. conceived the study. B.D.G. and T.B. wrote the manuscript with contributions from other authors.

FUNDING

University Medical Center Giessen and Marburg (UKGM); Prize of the Justus Liebig University Giessen (to B.D.G.); T.B. is supported by the Deutsche Forschungsgemeinschaft (DFG, German Research Foundation) [TRR81-A12 and BO 1639/9-1]; the State of Hesse (LOEWE iCANx), von Behring-Röntgen Stiftung [65-0004] and the Excellence Cluster for Cardio Pulmonary System (ECCPS) in Giessen. Funding for open access charge: DFG collaborative research [TRR81].
Conflict of interest statement. None declared.

REFERENCES

1. Aster,J.C., Pear,W.S. and Blacklow,S.C. (2017) The varied roles of notch in cancer. *Annu. Rev. Pathol.*, **12**, 245–275.
2. Allen,F. and Maillard,I. (2021) Therapeutic targeting of notch signaling: from cancer to inflammatory disorders. *Front. Cell Dev. Biol.*, **9**, 649205.
3. Parmigiani,E., Taylor,V. and Giachino,C. (2020) Oncogenic and tumor-suppressive functions of NOTCH signaling in glioma. *Cells*, **9**, 2304.
4. Borggrefe,T. and Oswald,F. (2009) The notch signaling pathway: transcriptional regulation at notch target genes. *Cell. Mol. Life Sci.*, **66**, 1631–1646.
5. Borggrefe,T., Lauth,M., Zwijsen,A., Huylebroeck,D., Oswald,F. and Giaimo,B.D. (2016) The notch intracellular domain integrates signals from wnt, hedgehog, TGFbeta/BMP and hypoxia pathways. *Biochim. Biophys. Acta*, **1863**, 303–313.
6. Antfolk,D., Antila,C., Kemppainen,K., Landor,S.K. and Sahlgren,C. (2019) Decoding the PTM-switchboard of notch. *Biochim. Biophys. Acta Mol. Cell. Res.*, **1866**, 118507.
7. Giaimo,B.D., Gagliani,E.K., Kovall,R.A. and Borggrefe,T. (2021) Transcription factor RBPJ as a molecular switch in regulating the notch response. *Adv. Exp. Med. Biol.*, **1287**, 9–30.
8. Giaimo,B.D., Ferrante,F., Vallejo,D.M., Hein,K., Gutierrez-Perez,I., Nist,A., Stiewe,T., Mittler,G., Herold,S., Zimmermann,T. *et al.* (2018) Histone variant H2A.Z deposition and acetylation directs the canonical notch signaling response. *Nucleic Acids Res.*, **46**, 8197–8215.
9. Oswald,F., Rodriguez,P., Giaimo,B.D., Antonello,Z.A., Mira,L., Mittler,G., Thiel,V.N., Collins,K.J., Tabaja,N., Cizelsky,W. *et al.* (2016) A phospho-dependent mechanism involving NCoR and KMT2D controls a permissive chromatin state at notch target genes. *Nucleic Acids Res.*, **44**, 4703–4720.
10. Xu,T., Park,S.S., Giaimo,B.D., Hall,D., Ferrante,F., Ho,D.M., Hori,K., Anhezini,L., Ertl,I., Bartkuhn,M. *et al.* (2017) RBPJ/CBF1 interacts with L3MBTL3/MBT1 to promote repression of notch signaling via histone demethylase KDM1A/LSD1. *EMBO J.*, **36**, 3232–3249.
11. Pillidge,Z. and Bray,S.J. (2019) SWI/SNF chromatin remodeling controls Notch-responsive enhancer accessibility. *EMBO Rep.*, **20**, e46944.
12. Di Stefano,L., Walker,J.A., Burgio,G., Corona,D.F., Mulligan,P., Naar,A.M. and Dyson,N.J. (2011) Functional antagonism between histone H3K4 demethylases in vivo. *Genes Dev.*, **25**, 17–28.
13. Mulligan,P., Yang,F., Di Stefano,L., Ji,J.Y., Ouyang,J., Nishikawa,J.L., Toiber,D., Kulkarni,M., Wang,Q., Najafi-Shoushtari,S.H. *et al.* (2011) A SIRT1-LSD1 corepressor complex regulates notch target gene expression and development. *Mol. Cell*, **42**, 689–699.
14. Yatim,A., Benne,C., Sobhian,B., Laurent-Chabalier,S., Deas,O., Judde,J.G., Lelievre,J.D., Levy,Y. and Benkirane,M. (2012) NOTCH1 nuclear interactome reveals key regulators of its transcriptional activity and oncogenic function. *Mol. Cell*, **48**, 445–458.
15. Yashiro-Ohtani,Y., Wang,H., Zang,C., Arnett,K.L., Bailis,W., Ho,Y., Knoechel,B., Lanauze,C., Louis,L., Forsyth,K.S. *et al.* (2014) Long-range enhancer activity determines myc sensitivity to notch inhibitors in t cell leukemia. *Proc. Natl. Acad. Sci. U.S.A.*, **111**, E4946–E4953.
16. Ryan,R.J.H., Petrovic,J., Rausch,D.M., Zhou,Y., Lareau,C.A., Kluk,M.J., Christie,A.L., Lee,W.Y., Tarjan,D.R., Guo,B. *et al.* (2017) A b cell regulome links notch to downstream oncogenic pathways in small b cell lymphomas. *Cell Rep.*, **21**, 784–797.
17. Wang,H., Zang,C., Taing,L., Arnett,K.L., Wong,Y.J., Pear,W.S., Blacklow,S.C., Liu,X.S. and Aster,J.C. (2014) NOTCH1-RBPJ complexes drive target gene expression through dynamic interactions with superenhancers. *Proc. Natl. Acad. Sci. U.S.A.*, **111**, 705–710.
18. Castel,D., Mourikis,P., Bartels,S.J., Brinkman,A.B., Tajbakhsh,S. and Stunnenberg,H.G. (2013) Dynamic binding of RBPJ is determined by notch signaling status. *Genes Dev.*, **27**, 1059–1071.
19. Yuan,Z., VanderWielen,B.D., Giaimo,B.D., Pan,L., Collins,C.E., Turkiewicz,A., Hein,K., Oswald,F., Borggrefe,T. and Kovall,R.A. (2019) Structural and functional studies of the RBPJ-SHARP complex reveal a conserved corepressor binding site. *Cell Rep.*, **26**, 845–854.
20. Giaimo,B.D., Ferrante,F. and Borggrefe,T. (2017) Chromatin immunoprecipitation (ChIP) in mouse T-cell lines. *J. Vis. Exp.*, **124**, 5907.
21. White,J., Blackman,M., Bill,J., Kappler,J., Marrack,P., Gold,D.P. and Born,W. (1989) Two better cell lines for making hybridomas expressing specific t cell receptors. *J. Immunol.*, **143**, 1822–1825.
22. van Essen,D., Dullforce,P., Brocker,T. and Gray,D. (2000) Cellular interactions involved in th cell memory. *J. Immunol.*, **165**, 3640–3646.
23. Ferrante,F., Giaimo,B.D., Bartkuhn,M., Zimmermann,T., Close,V., Mertens,D., Nist,A., Stiewe,T., Meier-Soelch,J., Kracht,M. *et al.* (2020) HDAC3 functions as a positive regulator in notch signal transduction. *Nucleic Acids Res.*, **48**, 3496–3512.
24. Collins,K.J., Yuan,Z. and Kovall,R.A. (2014) Structure and function of the CSL-KyoT2 corepressor complex: a negative regulator of notch signaling. *Structure*, **22**, 70–81.
25. Sanjana,N.E., Shalem,O. and Zhang,F. (2014) Improved vectors and genome-wide libraries for CRISPR screening. *Nat. Methods*, **11**, 783–784.
26. Reimers,M. and Carey,V.J. (2006) Bioconductor: an open source framework for bioinformatics and computational biology. *Methods Enzymol.*, **411**, 119–134.
27. TW,H.B. and Girke,T. (2016) systemPipeR: NGS workflow and report generation environment. *BMC Bioinf.*, **17**, 388.
28. Trapnell,C., Pachter,L. and Salzberg,S.L. (2009) TopHat: discovering splice junctions with RNA-Seq. *Bioinformatics*, **25**, 1105–1111.
29. Lawrence,M., Huber,W., Pages,H., Aboyoun,P., Carlson,M., Gentleman,R., Morgan,M.T. and Carey,V.J. (2013) Software for computing and annotating genomic ranges. *PLoS Comput. Biol.*, **9**, e1003118.
30. Love,M.I., Huber,W. and Anders,S. (2014) Moderated estimation of fold change and dispersion for RNA-seq data with DESeq2. *Genome Biol.*, **15**, 550.
31. Yu,G., Wang,L.G., Han,Y. and He,Q.Y. (2012) clusterProfiler: an r package for comparing biological themes among gene clusters. *OMICS*, **16**, 284–287.
32. Zhou,Y., Zhou,B., Pache,L., Chang,M., Khodabakhshi,A.H., Tanaseichuk,O., Benner,C. and Chanda,S.K. (2019) Metascape provides a biologist-oriented resource for the analysis of systems-level datasets. *Nat. Commun.*, **10**, 1523.
33. Romero-Wolf,M., Shin,B., Zhou,W., Koizumi,M., Rothenberg,E.V. and Hosokawa,H. (2020) Notch2 complements notch1 to mediate inductive signaling that initiates early t cell development. *J. Cell Biol.*, **219**, e202005093.
34. George,J., Lim,J.S., Jang,S.J., Cun,Y., Ozretic,L., Kong,G., Leenders,F., Lu,X., Fernandez-Cuesta,L., Bosco,G. *et al.* (2015) Comprehensive genomic profiles of small cell lung cancer. *Nature*, **524**, 47–53.
35. Severson,E., Arnett,K.L., Wang,H., Zang,C., Taing,L., Liu,H., Pear,W.S., Shirley Liu,X., Blacklow,S.C. and Aster,J.C. (2017) Genome-wide identification and characterization of notch transcription complex-binding sequence-paired sites in leukemia cells. *Sci. Signal*, **10**, eaag1598.
36. Davis,S. and Meltzer,P.S. (2007) GEOquery: a bridge between the gene expression omnibus (GEO) and bioconductor. *Bioinformatics*, **23**, 1846–1847.
37. Ritchie,M.E., Phipson,B., Wu,D., Hu,Y., Law,C.W., Shi,W. and Smyth,G.K. (2015) limma powers differential expression analyses for RNA-sequencing and microarray studies. *Nucleic Acids Res.*, **43**, e47.
38. Dieguez-Hurtado,R., Kato,K., Giaimo,B.D., Nieminen-Kelha,M., Arf,H., Ferrante,F., Bartkuhn,M., Zimmermann,T., Bixel,M.G., Eilken,H.M. *et al.* (2019) Loss of the transcription factor RBPJ induces disease-promoting properties in brain pericytes. *Nat. Commun.*, **10**, 2817.
39. Langmead,B. and Salzberg,S.L. (2012) Fast gapped-read alignment with bowtie 2. *Nat. Methods*, **9**, 357–359.
40. Kim,D., Langmead,B. and Salzberg,S.L. (2015) HISAT: a fast spliced aligner with low memory requirements. *Nat. Methods*, **12**, 357–360.
41. Feng,X., Grossman,R. and Stein,L. (2011) PeakRanger: a cloud-enabled peak caller for chip-seq data. *BMC Bioinf.*, **12**, 139.
42. Zhang,Y., Liu,T., Meyer,C.A., Eeckhoute,J., Johnson,D.S., Bernstein,B.E., Nusbaum,C., Myers,R.M., Brown,M., Li,W. *et al.* (2008) Model-based analysis of chip-Seq (MACS). *Genome Biol.*, **9**, R137.

43. Jalili,V., Matteucci,M., Masseroli,M. and Morelli,M.J. (2015) Using combined evidence from replicates to evaluate chip-seq peaks. *Bioinformatics*, **31**, 2761–2769.
44. Amemiya,H.M., Kundaje,A. and Boyle,A.P. (2019) The ENCODE blacklist: identification of problematic regions of the genome. *Sci. Rep.*, **9**, 9354.
45. Ramirez,F., Dundar,F., Diehl,S., Gruning,B.A. and Manke,T. (2014) deepTools: a flexible platform for exploring deep-sequencing data. *Nucleic Acids Res.*, **42**, W187–W191.
46. Yu,G., Wang,L.G. and He,Q.Y. (2015) ChIPseeker: an R/Bioconductor package for ChIP peak annotation, comparison and visualization. *Bioinformatics*, **31**, 2382–2383.
47. Lun,A.T. and Smyth,G.K. (2016) csaw: a bioconductor package for differential binding analysis of chip-seq data using sliding windows. *Nucleic Acids Res.*, **44**, e45.
48. Hahne,F. and Ivanek,R. (2016) Visualizing genomic data using gviz and bioconductor. *Methods Mol. Biol.*, **1418**, 335–351.
49. Ernst,J. and Kellis,M. (2012) ChromHMM: automating chromatin-state discovery and characterization. *Nat. Methods*, **9**, 215–216.
50. Oswald,F., Tauber,B., Dobner,T., Bourteele,S., Kostezka,U., Adler,G., Liptay,S. and Schmid,R.M. (2001) p300 acts as a transcriptional coactivator for mammalian Notch-1. *Mol. Cell. Biol.*, **21**, 7761–7774.
51. Rozenberg,J.M., Taylor,J.M. and Mack,C.P. (2018) RBPJ binds to consensus and methylated cis elements within phased nucleosomes and controls gene expression in human aortic smooth muscle cells in cooperation with SRF. *Nucleic Acids Res.*, **46**, 8232–8244.
52. Adler,S.H., Chiffoleau,E., Xu,L., Dalton,N.M., Burg,J.M., Wells,A.D., Wolfe,M.S., Turka,L.A. and Pear,W.S. (2003) Notch signaling augments t cell responsiveness by enhancing CD25 expression. *J. Immunol.*, **171**, 2896–2903.
53. Jarrett,S.M., Seegar,T.C.M., Andrews,M., Adelmant,G., Marto,J.A., Aster,J.C. and Blacklow,S.C. (2019) Extension of the notch intracellular domain ankyrin repeat stack by NRARP promotes feedback inhibition of notch signaling. *Sci. Signal*, **12**, eaay2369.
54. Lamar,E., Deblandre,G., Wettstein,D., Gawantka,V., Pollet,N., Niehrs,C. and Kintner,C. (2001) Nrarp is a novel intracellular component of the notch signaling pathway. *Genes Dev.*, **15**, 1885–1899.
55. Yun,T.J. and Bevan,M.J. (2003) Notch-regulated ankyrin-repeat protein inhibits notch1 signaling: multiple notch1 signaling pathways involved in t cell development. *J. Immunol.*, **170**, 5834–5841.
56. Izon,D.J., Aster,J.C., He,Y., Weng,A., Karnell,F.G., Patriub,V., Xu,L., Bakkour,S., Rodriguez,C., Allman,D. *et al.* (2002) Deltex1 redirects lymphoid progenitors to the b cell lineage by antagonizing notch1. *Immunity*, **16**, 231–243.
57. Singh,S.B., Coffman,C.N., Carroll-Portillo,A., Varga,M.G. and Lin,H.C. (2021) Notch signaling pathway is activated by sulfate reducing bacteria. *Front. Cell Infect. Microbiol.*, **11**, 695299.
58. Wang,X., Sun,L., Zhang,L. and Jiang,Z. (2016) Effect of adoptive transfer or depletion of regulatory t cells on Triptolide-induced liver injury. *Front. Pharmacol.*, **7**, 99.
59. Croom,H.A., Izon,D.J., Chong,M.M., Curtis,D.J., Roberts,A.W., Kay,T.W., Hilton,D.J., Alexander,W.S. and Starr,R. (2008) Perturbed thymopoiesis in vitro in the absence of suppressor of cytokine signalling 1 and 3. *Mol. Immunol.*, **45**, 2888–2896.
60. Wilson,A., MacDonald,H.R. and Radtke,F. (2001) Notch 1-deficient common lymphoid precursors adopt a b cell fate in the thymus. *J. Exp. Med.*, **194**, 1003–1012.
61. Radtke,F., Wilson,A., Stark,G., Bauer,M., van Meerwijk,J., MacDonald,H.R. and Aguet,M. (1999) Deficient t cell fate specification in mice with an induced inactivation of notch1. *Immunity*, **10**, 547–558.
62. Bian,W., Tang,M., Jiang,H., Xu,W., Hao,W., Sui,Y., Hou,Y., Nie,L., Zhang,H., Wang,C. *et al.* (2021) Low-density-lipoprotein-receptor-related protein 1 mediates notch pathway activation. *Dev. Cell*, **56**, 2902–2919.
63. Meng,H., Zhang,X., Lee,S.J., Strickland,D.K., Lawrence,D.A. and Wang,M.M. (2010) Low density lipoprotein receptor-related protein-1 (LRP1) regulates thrombospondin-2 (TSP2) enhancement of notch3 signaling. *J. Biol. Chem.*, **285**, 23047–23055.
64. Lin,S., Sun,L., Lyu,X., Ai,X., Du,D., Su,N., Li,H., Zhang,L., Yu,J. and Yuan,S. (2017) Lactate-activated macrophages induced aerobic glycolysis and epithelial-mesenchymal transition in breast cancer by regulation of CCL5-CCR5 axis: a positive metabolic feedback loop. *Oncotarget*, **8**, 110426–110443.
65. Wang,X., Shen,Q.W., Wang,J., Zhang,Z., Feng,F., Chen,T., Zhang,Y., Wei,H., Li,Z., Wang,X. *et al.* (2016) KLF7 regulates satellite cell quiescence in response to extracellular signaling. *Stem Cells*, **34**, 1310–1320.
66. Bai,J., Khajavi,M., Sui,L., Fu,H., Tarakkad Krishnaji,S., Birsner,A.E., Bazinet,L., Kamm,R.D. and D'Amato,R.J. (2021) Angiogenic responses in a 3D micro-engineered environment of primary endothelial cells and pericytes. *Angiogenesis*, **24**, 111–127.
67. Han,H., Tanigaki,K., Yamamoto,N., Kuroda,K., Yoshimoto,M., Nakahata,T., Ikuta,K. and Honjo,T. (2002) Inducible gene knockout of transcription factor recombination signal binding protein-J reveals its essential role in t versus b lineage decision. *Int. Immunol.*, **14**, 637–645.
68. Pitulescu,M.E., Schmidt,I., Giaimo,B.D., Antoine,T., Berkenfeld,F., Ferrante,F., Park,H., Ehling,M., Biljes,D., Rocha,S.F. *et al.* (2017) Dll4 and notch signalling couples sprouting angiogenesis and artery formation. *Nat. Cell Biol.*, **19**, 915–927.
69. Diaz-Trelles,R., Scimia,M.C., Bushway,P., Tran,D., Monosov,A., Monosov,E., Peterson,K., Rentschler,S., Cabrales,P., Ruiz-Lozano,P. *et al.* (2016) Notch-independent RBPJ controls angiogenesis in the adult heart. *Nat. Commun.*, **7**, 12088.
70. Kulic,I., Robertson,G., Chang,L., Baker,J.H., Lockwood,W.W., Mok,W., Fuller,M., Fournier,M., Wong,N., Chou,V. *et al.* (2015) Loss of the notch effector RBPJ promotes tumorigenesis. *J. Exp. Med.*, **212**, 37–52.